IJIE

UTHM Penerbit

INTERNATIONAL JOURNAL OF INTEGRATED ENGINEERING
ISSN: 2229-838X e-ISSN: 2600-7916

Vol. 18 No. 2 (2026) 278-293
https://publisher.uthm.edu.my/ojs/index.php/ijie

Numerical Study on the Effect of Glazing Layer on the Performance of a Flat Plate Solar Collector

Akeef Mursyidiy[1], Syed Noh Syed Abu Bakar[1]*, Mohammad Jamil Ahmad[2], Mohd Azan Mohammed Sapardi[1], Sany Izan Ihsan[1]

[1] *Department of Mechanical and Aerospace Engineering, Kulliyyah of Engineering, International Islamic University Malaysia (IIUM), Gombak, 53100, MALAYSIA*

[2] *Department of Mechanical Engineering, Aligarh Muslim University, Aligarh-202002, UP, INDIA*

*Corresponding Author: syednoh@iium.edu.my
DOI: https://doi.org/10.30880/ijie.2026.18.02.022

Article Info

Received: 15 November 2025
Accepted: 31 March 2026
Available online: 16 June 2026

Keywords

Flat plate solar collector, number of glazing layers, absorber plate temperature, top heat loss coefficient

Abstract

The glazing or glass cover is a key component of a flat plate solar collector (FPSC), influencing both thermal and optical performance. This study investigates the effect of varying the number of glazing layers (1 to 4) on the absorber plate temperature and top heat loss coefficient. Results show that the 2-glazing layer configuration yields the highest absorber temperature at 376.48 K, but also a relatively higher top heat loss coefficient, U_t, compared to the 3 and 4-glazing layer configurations. The top heat loss coefficient shows a diminishing decline as more glazing layers are added. Adding glazing layers introduces a greenhouse effect by transmitting solar short-wave radiation while trapping long-wave heat, which enhances FPSC thermal retention but slightly reduces surface incident radiation due to optical losses. The 2-glazing configuration yields the highest absorber temperature due to its balance between U_t and surface incident radiation. These findings provide insight for optimizing glazing configurations in solar collector design.

1. Introduction

The increasing global demand for energy, coupled with environmental concerns over fossil fuel consumption, has accelerated the development of renewable energy technologies. Among these, solar energy offers considerable advantages due to its abundance, environmental friendliness, and potential for both large-scale and decentralized applications, making it promising renewable energy sources for addressing global energy challenges and reducing carbon emissions [1-3].

Significant advancements have been made in solar thermal technologies, enabling their application at both industrial and domestic scales. High-performance collectors such as parabolic trough collectors (PTC), parabolic dish reflectors (PDR), and compound parabolic collectors (CPC) are capable of delivering the high operating temperatures (333.15 K to 773.15 K) required for industrial processes such as drying, sterilization, and polymerization [4-6]. For residential and small-scale applications, flat plate solar collectors (FPSC) and evacuated tube collectors (ETC) are more common due to their simplicity, affordability, and suitability for low to moderate temperature applications such as space and water heating [7-9].

The FPSC is one of the most widely adopted solar thermal technologies due to its simple design, low manufacturing cost, and reliable performance. In an FPSC, solar radiation passes through a transparent cover, known as glazing, and is absorbed by a dark-colored absorber plate, which transfers heat to a working fluid circulating within the collector [10]. Fig. 1 shows a simplified schematic of an FPSC, highlighting the key processes of solar energy interaction within the collector. Incoming solar radiation partially reflects off the glazing layer, while the transmitted portion reaches the absorber plate through the transparent glazing and air gap. The absorber plate captures the transmitted solar radiation and converts it into heat, which is then transferred to the fluid inside the tubes. Thermal losses occur mainly through the top glazing by means of convection and radiation.

An important factor in evaluating the performance of these collectors is surface incident radiation, which is defined as the solar energy per unit area that reaches the collector's surface in the context of FPSC (measured in W/m^2). This encompasses direct radiation, diffused radiation, and reflected radiation from the ground and surroundings, including the component within the FPSC itself. Understanding and quantifying surface incident radiation matters because it directly influences how much energy the absorber can capture and convert with minimal losses [7]. It can be affected by several factors, such as orientation and tilt, where collectors are oriented relative to the sun to affect the incidence angle, since the solar flux on the surface is scaled by the cosine of this angle. This factor was studied extensively by Idowu and Olarenwaju [11], Kocer et al. [12]and Lv et al. [13], who focus on how orientation and tilt affect the performance of FPSC in terms of deviation from optimal orientation and monthly or yearly tilt adjustment for optimising the performance in various geographic locations.

Glazing is a critical component of FPSCs, serving protective and thermal functions. It protects the absorber and other internal components from environmental exposure while reducing heat loss by limiting convective and radiative losses through the top surface [14]. However, the glazing also affects the optical transmittance of solar radiation or short-wave radiation. Therefore, an optimal glazing design must balance improved thermal insulation with minimal optical losses [15-21].

Additionally, the greenhouse effect can occur inside FPSC once the glazing layer is introduced, as it also traps and re-radiates back some of the thermal (long-wave) radiation emitted from the absorber plate, and the inner glazing effectively redirects more energy back toward the absorber. This phenomenon can affect the surface incident radiation on the absorber plate and glazing as additional glazing layers are introduced [22].

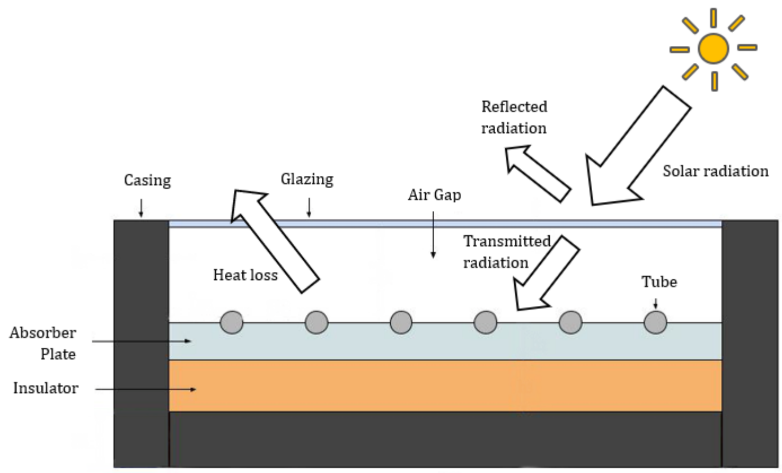

Fig. 1 *Schematic diagram of an FPSC, showing the main components and solar radiation interactions*

Previous studies have shown that increasing the number of glazing layers can significantly affect the thermal performance of FPSCs. For instance, Ihaddadene et al. [19] reported reduced collector efficiency with double glazing under artificial light conditions, attributing the performance drop to increased air gaps that act as thermal insulators but reduce transmitted energy to the working fluid. In contrast, Al-Ajlan et al. [23] demonstrated that under moderate operating temperatures, the benefits of reduced heat loss due to multiple glazing layers can outweigh the reduction in optical efficiency, leading to higher outlet fluid temperatures. An experimental study by Sarma et al. [21] reported that the double-glazing configuration achieved the highest stagnation temperature when there was no heat withdrawal from the absorber plate. Chen et al. [24] further explored the role of double-glazing configurations filled with air, argon, or vacuum, highlighting the reduction in convective heat losses. A study by M. Ameri et al. [25] reported that double glazing configurations exhibit higher thermal performance, resulting from reduced convective and radiative heat loss. However, they also noted that under low solar irradiation and lower absorber temperatures, additional layers can hinder performance due to reduced solar transmittance. Arasteh et al. [26] stated that adding more gaps via glazing layers can reduce the overall heat transfer coefficient by suppressing natural convection, but the law of diminishing returns will take effect. The study performed by Nassar et al. [27] highlighted that a higher number of glazing layers resulted in better performance in terms of useful heat gain when the temperature differential between the absorber plate and ambient air is higher. Givi et al. [28] highlighted that the double-glazing configuration consistently outperforms the single-glazing design, especially in smaller air gaps, due to reduced turbulence and heat loss. As the air gap increases, the efficiency difference decreases, indicating that the insulation effect becomes more significant, decreasing the advantage of the double-glazing design.

Glazing thickness has a significant impact on FPSC performance due to its influence on solar transmittance and thermal insulation. Studies by Bakari et al. [16] and Liu et al. [29] consistently identified 4 mm glass as optimal, offering the best balance between high transmittance and reduced convective losses. Thinner glazing allows greater solar transmission but suffers from higher heat loss, while thicker glazing reduces convective loss but reduces incoming solar radiation due to increased reflectivity and insulation. Further supporting these findings, an experimental study from Singh et al. [30] shows that 4mm glass thickness performed best during the daytime when compared with 2 , 3 and 5 mm glazing thickness. However, Harun et al. [31] reported that a 2-mm glazing thickness yielded the highest total heat gain, while further increases in thickness resulted in reduced heat gain due to lower solar transmittance. Wang et al. [32] study on the FPSC utilizing flat micro heat pipe arrays reported that the optimal glass thickness of 3 mm and the air gap thickness of 35 mm yield improved thermal insulation.

Maintaining an optimal air gap between the absorber and glazing is critical for the performance of FPSC. Studies by Nahar and Garg [33] and Nahar and Gufta [34] found that a 50 mm gap minimizes convective losses and shading effects compared to 25 mm and 150 mm gaps. They recommend a 40 to 50-mm air gap for both the absorber-to-glazing and glazing-to-glazing spacing to achieve optimal thermal performance. In contrast, Pourfayaz et al. [35] outlined an increase in the air gap between the absorber and glazing results in a decrease in the heat loss coefficient, with this reduction being most pronounced up to a spacing of approximately 20 to 25 mm, beyond which further increases in spacing have a negligible effect on the top heat loss coefficient of the collector. A numerical study by Wenceslas Koholé et al. [36] reported that as the gap spacing between the collector absorber and the glazing increased from 0 to 40 mm, the irreversibility rate of the absorber plate, as well as the energy and exergy efficiencies, increased, while the irreversibility rate of the glazing decreased. Beyond a separation of 40 mm, the impact on the system's performance became minimal. Mekahlia et al. [37] noted that thinner gaps (1 to 8 mm) primarily conducted heat, while thicker gaps increased natural convection, raising thermal losses. They added that adding a second glazing reduced convection, enhancing collector temperature and decreasing thermal loss.

Despite these contributions, most existing studies have focused primarily on single and double-glazing configurations. The impact of incorporating more than two glazing layers on thermal efficiency and heat transfer characteristics remains inadequately explored. Furthermore, understanding the distribution of convective and radiative heat transfer through multiple glazing layers is essential for optimizing FPSC design, especially in regions with high ambient temperatures such as Malaysia.

Therefore, this study investigates the effect of varying the number of glazing layers, from one to four, on the thermal performance of flat plate solar collectors. Using a combination of Computational Fluid Dynamics (CFD) and analytical modeling, this work analyzes absorber plate temperature, the convective and radiative heat transfer coefficient and the top heat loss coefficient. The results provide insights into the optimal glazing configuration for enhancing FPSC efficiency while minimizing heat loss.

2. Problem Description

The physical domain being analysed is the upper section of an FPSC, specifically from the absorber plate top to the glazing. This domain was chosen to focus on the temperature and the top heat loss occurring at the absorber plate across various configurations. It was assumed that the collector operates under steady-state conditions, and the effects of ambient temperature and solar irradiation were considered uniform across the surface. An emissivity of unity was assumed for the absorber plate ($\varepsilon_g = 1$) and the glazing ($\varepsilon_p = 1$) to simplify radiation analysis and ensure consistent comparison across all glazing configurations. The transmittance of glass was determined using its refractive index, which was set to 1.5 to represent common glazing properties of FPSC. The ambient was assumed to have a constant convective heat transfer coefficient of 5 $W \cdot m^{-2} \cdot K^{-1}$, representing the convection in calm air. The Boussinesq approximation was applied for air in the air gap, assuming moderate temperature variations are within acceptable limits for natural convection modelling and faster convergence. The sides and bottom of the domain were assumed to be adiabatic so that heat can be lost only from the top surface of the glazing. The ambient temperature was assumed to be 303.15 K. These assumptions and considerations were made to isolate the influence of glazing on the top heat loss and absorber plate average temperature. The top heat loss and absorber plate temperature represent thermal performance, as one can argue that the lower top heat loss and higher absorber plate temperature would lead to higher thermal performance of the FPSC.

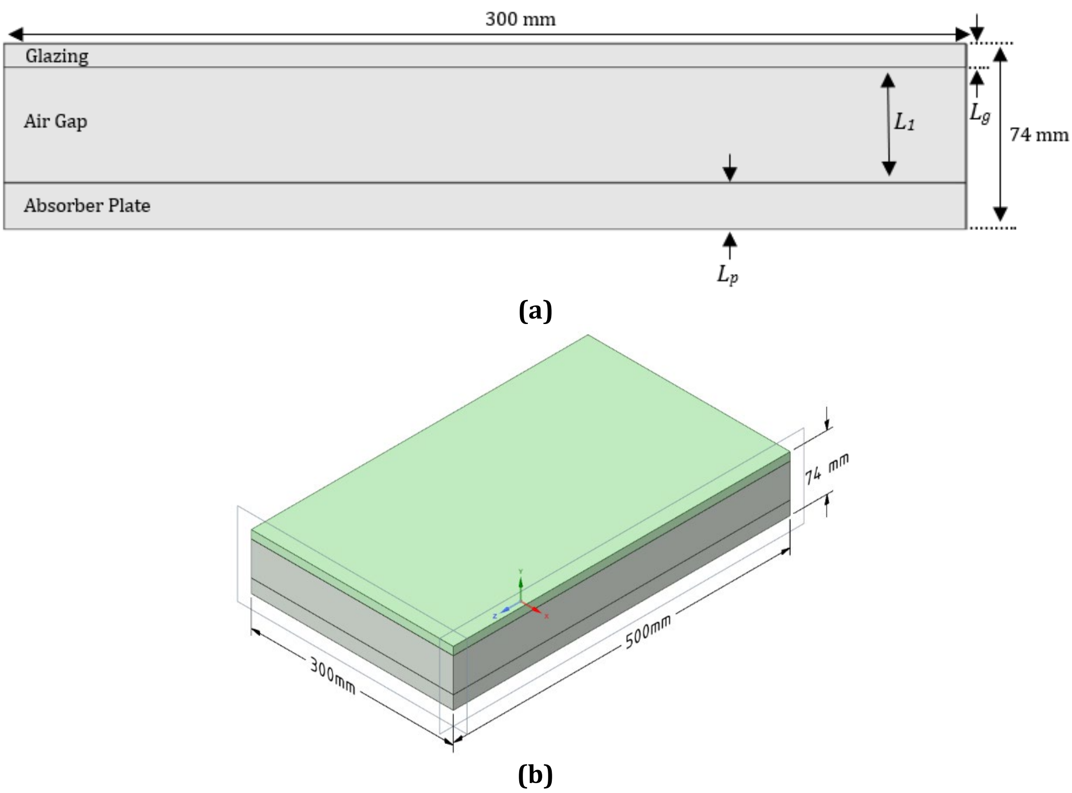

Fig. 2 *Physical domain for 1 glazing layer. (a) Is he front view of the domain; and (b) Is the isometric view of the domain*

The illustration of the physical domain is shown in Fig. 2. The size of the physical domain for the 1-glazing configuration is 500 mm length × 300 mm width × 74 mm height, consisting of glazing, air and absorber plate. The glazing and absorber plate thicknesses are 4 mm and 20 mm, respectively. The gap between the absorber plate and glazing is 50 mm. The length and width of the absorber plate, air gap and glazing are the same. For 2, 3 and 4 glazing configurations, the gap spacing and the glazing thickness are added accordingly, while the dimension is maintained as the gap spacing and glazing thickness for 1 glazing configuration. The geometrical parameters of the domain from Fig. 2 are tabulated in Table 1 with their values. Table 2 shows the material and properties of the components in the FPSC model.

Table 1 *The geometrical parameters for the top part of the FPSC model*

Geometrical Parameters	Value
Glazing thickness, L_g	4-mm
Absorber plate thickness, L_p	20-mm
Air gap spacing between the absorber plate and the first glazing, L_1	50-mm
Air gap spacing between the first glazing and the second glazing, L_2	50-mm
Air gap spacing between the second glazing and the third glazing, L_3	50-mm
Air gap spacing between the third glazing and the fourth glazing, L_4	50-mm

In this study, the parameters of the number of glazing layers were systematically varied to study their influence on the temperature of the absorber plate and the top heat-loss coefficient, Ut, of the top part of the FPSC. With the addition of a glazing layer, an extra set of thermal resistances is introduced between the absorber plate and the ambient environment. Convection and radiation across the air gaps, along with conduction through the glazing material, are accounted for in the formation of the total thermal resistance from the absorber to the outermost glazing. The value of U_t is then determined as the inverse of this total thermal resistance.

To obtain the value of U_t for the single glazing configuration, the equation from U_t obtained from Samdarshi & Mullick [38] was used:

$$U_t = \left[\left(h_{cpg1} + h_{rpg1}\right)^{-1} + \left(h_w + h_{rg1a}\right)^{-1} + \frac{L_g}{k_g}\right]^{-1} \tag{1}$$

where h_w is the convective heat transfer coefficient of the ambient, which is assumed at 5 W·m^{-2}·K^{-1}, L_g is the thickness of the glazing and k_g is the thermal conductivity of glazing. The number subscript 1 refers to glazing layer 1 (the closest to the absorber). For the subsequent layer, the number is increased accordingly.

The value of h_{cpg1}, h_{rpg1}, h_{rg1a} was calculated by Bisen et al. [39]:

$$h_{cpg1} = \frac{K_1 \times N_{u1}}{L_1} \tag{2}$$

$$h_{rpg1} = \left\{\frac{\sigma}{\frac{L_1}{\varepsilon_p} + \frac{1}{\varepsilon_g} - 1}\right\}\left(T_p^2 + T_{g1}^2\right)\left(T_p + T_{g1}\right) \tag{3}$$

$$h_{rg1a} = \sigma \cdot \varepsilon_g \frac{\left(T_{g1}^4 - T_{sky}^4\right)}{T_{g1} - T_a} \tag{4}$$

The σ is the Stefan–Boltzmann constant (σ = 5.67 × 10^8). The T_{sky} was calculated using the equation from Swinbank [40]:

$$T_{sky} = 0.0552 \times T_a^{1.5} \tag{5}$$

Where the ambient temperature, T_a is set as 303.15 K.

The thermal conductivity of air, K_1 is the kinematic viscosity of air, V_1 and is the Prandtl number of the air, P_{r1} were evaluated at the arithmetic mean surface temperature of the layer between absorber plate and first glazing, T_{m1}. Their correlations were given by Bisen et al. [39]:

$$K_1 = -3 \times 10^{-8}\, T_{m1}^2 + 10^{-4} T_{m1} 4 \times 10^{-5} T_{m1} \tag{6}$$

$$V_1 = -(9 \times 10^{-5} T_{m1}^2 + 0.04 T_{m1} - 4.17) \times 10^{-6} \tag{7}$$

$$P_{r1} = +1.057 - 0.06 log T_{m1} \tag{8}$$

Since this study focuses only on the influence of the number of glazing layers, the tilt angle, τ of FPSC is set as 0°, so the R_{a1} cos 0° = R_{a1} [41]. The value of N_{u1} was calculated using the following equations that depend on the obtained value of R_{a1} by [41]:

$$N_{u1} = 1 + 1.446\left(1 - \frac{1708}{R_{a1}}\right) \quad \text{for } 1708 < R_{a1} < 5900 \tag{9}$$

$$N_{u1} = 0.229 \times R_{a1}^{0.252} \quad \text{for } 5900 < R_{a1} < 9.23 \times 10^4 \tag{10}$$

$$N_{u1} = 0.157 \times R_{a1}^{0.285} \quad \text{for } 9.23 \times 10^4 < R_{a1} < 10^6 \tag{11}$$

The value of R_{a1} was obtained by using [39]:

$$R_{a1} = \frac{9.8 \times \left(T_p - T_{g1}\right)(L_1)^3 (P_{r1})}{V_1^2 \left(\frac{T_p + T_{g1}}{2}\right)} \tag{12}$$

For each configuration, simulations were performed in ANSYS Fluent to determine the average surface temperatures of the absorber plate, T_p and of each glazing layer (T_{g1}, T_{g2}, T_{g3}, T_{g4}). The average temperature of the absorber plate and each glazing will be determined using the surface integral report function of area-weighted average from ANSYS Fluent. Since the convective and radiative heat transfer are highly dependent on temperature and affect the U_t, the layer's mean temperature, T_m, was calculated to evaluate air properties and thus accurately determine convective, hc and radiative, hr heat transfer coefficients. These temperatures were used to calculate the arithmetic mean of the corresponding surface temperature (T_m) based on this equation [39]:

$$T_m = \frac{T_p + T_g}{2} \tag{13}$$

Equation (13) was applied to the layer between the absorber plate and the first glazing, and this equation was also applied to the subsequent layers, such as the layer between the first and second glazing, and so forth. Consequently, for the layer between the absorber and first glazing, the T_{m1} was calculated, then, for the layer between the first and second glazing, T_{m2} was calculated, and so on for the next layers.

For the 2-, 3- and 4-glazing configuration, the corresponding convective and radiative heat transfer coefficients for subsequent layers were calculated using Equations (2) and (3). For example, for the second layer of 2-glazing configuration, the convective heat transfer coefficient, h_{cg1g2} and radiative heat transfer coefficient, h_{rg1g2} were calculated using [39]:

$$h_{cg1g2} = \frac{K_2 \times N_{u2}}{L_2} \tag{14}$$

$$h_{rg1g2} = \left\{ \frac{\sigma}{\frac{L_2}{\varepsilon_p} + \frac{1}{\varepsilon_g} - 1} \right\} \left(T_{g1}^2 + T_{g2}^2\right)\left(T_{g1} + T_{g2}\right) \tag{15}$$

For the 2-, 3- and 4-glazing configuration, the equation of convective and radiative heat transfer coefficient for the subsequent glazing layer (second, third and fourth glazing layer) were taken into consideration for the U_t equation, extending the formula of U_t as shown below. The equation of U_t for 2-glazing layer configuration is obtained from Mullick and Samdarshi [42]:

$$U_t = \left[\left(h_{cpg1} + h_{rpg1}\right)^{-1} + \left(h_{cg1g2} + h_{rg1g2}\right)^{-1} + \left(h_w + h_{rg2a}\right)^{-1} + \frac{2L_g}{k_g} \right]^{-1} \tag{16}$$

For 3- and 4-glazing layer configurations, the equation of U_t will be extended to account for additional third and fourth glazing as the following:

$$U_t = \left[\left(h_{cpg1} + h_{rpg1}\right)^{-1} + \left(h_{cg1g2} + h_{rg1g2}\right)^{-1} + \left(h_{cg2g3} + h_{rg2g3}\right)^{-1} + \left(h_w + h_{rg3a}\right)^{-1} + \frac{3L_g}{k_g} \right]^{-1} \tag{17}$$

$$\begin{aligned} U_t = \Big[&\left(h_{cpg1} + h_{rpg1}\right)^{-1} + \left(h_{cg1g2} + h_{rg1g2}\right)^{-1} + \left(h_{cg2g3} + h_{rg2g3}\right)^{-1} \\ &+ \left(h_{cg3g4} + h_{rg3g4}\right)^{-1} + \left(h_w + h_{rg4a}\right)^{-1} + \frac{4L_g}{k_g} \Big]^{-1} \end{aligned} \tag{18}$$

2.1 Simulation Setup

A constant solar radiation load was applied to the physical domain using the Solar Load Model in ANSYS Fluent. The wall boundary condition for absorber was set to “mixed” (convection and radiation) with the surrounding temperature set at 303.15 K, heat transfer coefficient was set at 5 W·m^{-2}·K^{-1}, emissivity of unity (black surface) and set as opaque. The glazing’s surface was given the same thermal boundary conditions as the absorber; however, their radiation boundary was set as semi-transparent to allow the radiation to pass through and for the most top glazing is exposed to ambient conditions, permitting heat loss through convection and radiation. The contact region of absorber and glazing with air domain was set to coupled, to allow the heat transfer between them. The air domain of each layer was set as participating in radiation. The casing or the side wall of the domain and the bottom of the absorber were set as adiabatic and opaque to eliminate heat loss through these boundaries. The air domain was modeled to participate in convective heat transfer between the absorber and the glazing layers. These boundary conditions ensure that heat loss occurs solely through the top surface, thus isolating the effect of the glazing configuration on top heat loss. These boundary conditions were summarized in Fig. 3.

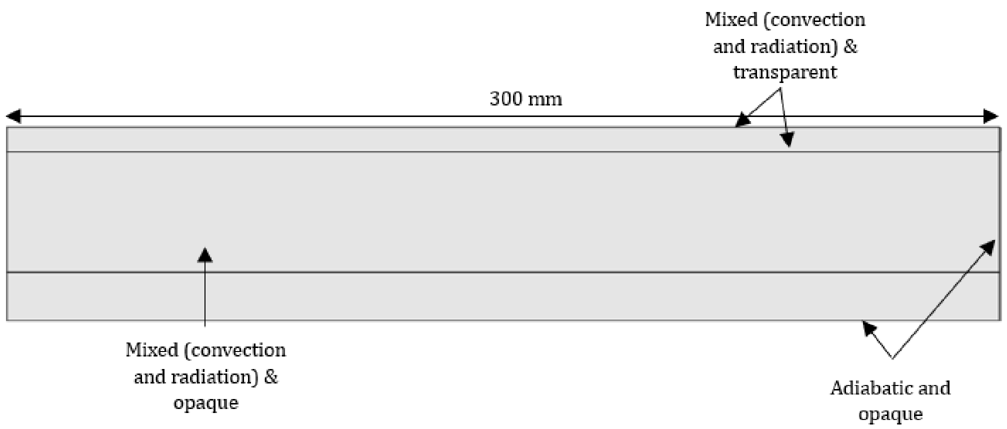

Fig. 3 *The boundary condition of the physical domain of FPSC*

In the solver setting, the energy equation was enabled. The standard k-epsilon model was selected for the viscous model due to its acceptable accuracy for heat transfer and flow simulations. Discrete Ordinates (DO) was selected as a radiation model as it enables the definition of semi-transparent interior and exterior walls in ANSYS Fluent, which is necessary to simulate radiation passing through glazing material. The solar load model used was solar irradiation with the longitude and latitude of Kuala Lumpur, Malaysia, at 1 p.m. The sun direction vector, direct solar irradiation and diffuse solar irradiation were calculated by the software, based on the global position and time given. The calculated value of direct irradiation was 874 W·m$^{-2,}$ and the diffuse irradiation was 102 W·m^{-2}. Both irradiations are used to simulate the FPSC receiving total solar radiation.

The second-order upwind scheme was used for spatial discretisation as it provides more accurate results, although at the cost of slower convergence. A summary of the physical models and solver configurations applied in ANSYS Fluent is presented in Table 3. The simulation was considered as converged when residuals of the energy, do-intensity and all other parameters are below the default setting criteria, which are 10^{-6}, 10^{-6} and 10^{-3}, respectively.

Table 2 *Configuration of numerical settings employed in ANSYS Fluent*

Simulation setting	Configuration
Energy equation	Enabled
Solver type	Pressure-Based
Time	Steady
Gravitational Acceleration	-9.81 m s^{-1} at *y*-direction
Viscous Model	Standard k-epsilon
Radiation Model	Discrete Ordinates (DO)
Solar Load Model	Solar Irradiation

The material properties used is shown in Table 2.

Table 3 *The material properties of the components in the FPSC model*

Material	Copper	Glass	Air
Density (kg m^{-3})	8933	2800	1.1644
Specific heat capacity, C_p (J kg^{-1} K^{-1})	385	750	1006.43
Thermal conductivity, k (W m^{-1} K^{-1})	401	0.7	0.0242

In Ansys Meshing, the mesh is created using the number of divisions function and a bias type of smaller divisions near the edge of the model to create a non-uniform and finer mesh near the wall boundary of the model for better prediction of heat transfer and fluid flow behavior. The number of elements in the mesh for all developed FPSC models ranges from 1.75 × 10^6 for the single-glazing model to 7.75 × 10^6 for the 4-glazing layer model, which is sufficient to achieve residual and energy convergence in the simulation. The applied mesh setting and refinement near the wall boundaries are shown in Fig. 4.

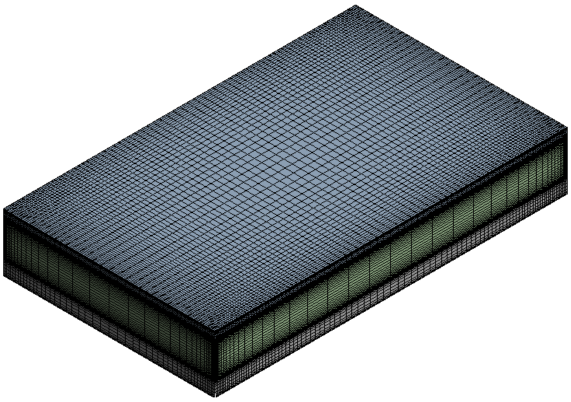

Fig. 4 *Mesh configuration of FPSC model*

2.2 Validation

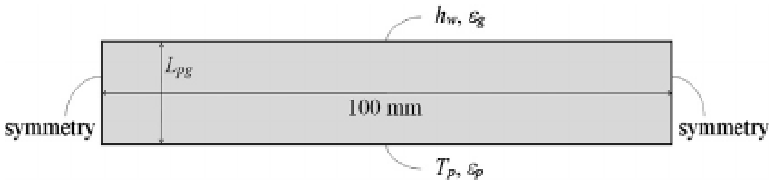

Fig. 5 *The physical domain of the single glazing FPSC 2-D model from Subiantoro & Ooi's study [43]*

To ensure the reliability of the simulation of this study, studies from Subiantoro and Ooi [43] and Wang et al. [44] were replicated and validated, following closely their reported configuration and parameters. First, the FPSC cases of Subiantoro and Ooi [43] was replicated to establish a 2-D and 3-D benchmark. The 2-D model of Subiantoro and Ooi's [43] as shown in Fig. 5, consists of 25 mm air gap, 100 mm length, symmetric side boundaries, laminar flow, the Surface-to-Surface (S2S) and the Discrete Ordinate (DO) radiation model, managed to converge smoothly and reproduced their temperature contours as shown in Fig. 6. Extending to a 3-D domain (25 mm × 100 mm × 500 mm) resulted in not achieving convergence as the residual stop dropping and begin stalling, but thermal metrics remained robust between the 2-D and 3-D domain, for both radiation model; the Nusselt number differed only by 4.08 % and the average plate temperature differed by only 0.3 %. Additionally, the energy balance verification showed minimal imbalance: 1.35404 ×10^{-6} W for the 2-D model and 0.00691 W for the 3-D model, confirming acceptable energy conservation as the net heat imbalance value is relatively small. The comparison of heat transfer and energy balance checks was summarised in Table 4.

Table 4 *Comparison of results of current works 2D and 3D, and Subiantoro & Ooi [43]*

Parameter	2-D Model	3-D Model	Subiantoro & Ooi's case [43]	% Error / Deviation
Nusselt Number (N_u)	10.3446	9.9223	-	4.08%
Energy Imbalance (W)	1.3540413 × 10^{-6}	0.00691	-	–
Top Surface Temperature (K)	319.32	318.36	317.80	0.48 % (2-D) 1.76 % (3-D)

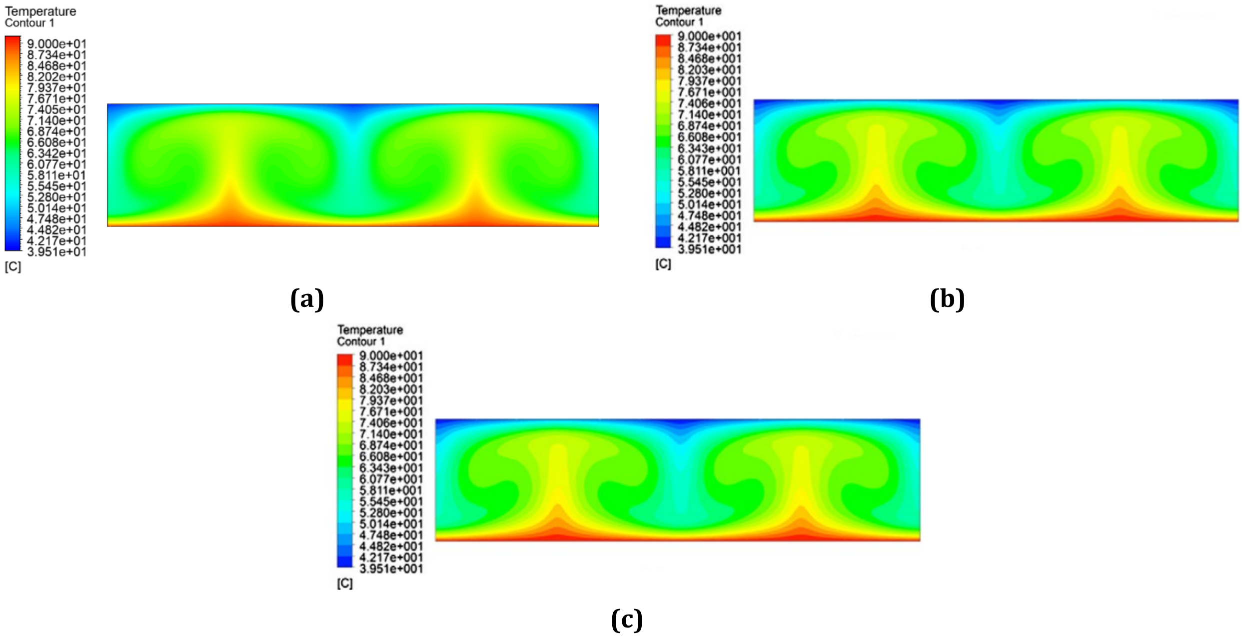

Fig. 6 *The comparison of the temperature contour of replicated 2-D model with S2S model) (a) with DO model; (b) and Subiantoro & Ooi's; (c) 2-D model [43]*

Since the residuals of the 3D FPSC were stalled before reaching the convergence criteria reported by Subiantoro & Ooi [43], the differentially heated cubical cavity of Wang et al. [44] as shown in Fig. 7, it was reproduced as a second 3D benchmark. Following the configuration and settings from Wang et al. [44], boundary conditions of a hot right wall, a cold left wall, and adiabatic remaining walls were applied, and a non-uniform mesh with near-wall refinement and constant fluid properties was employed in ANSYS Fluent to replicate both the non-radiation, the S2S and DO radiation model cases from Wang et al. [44].

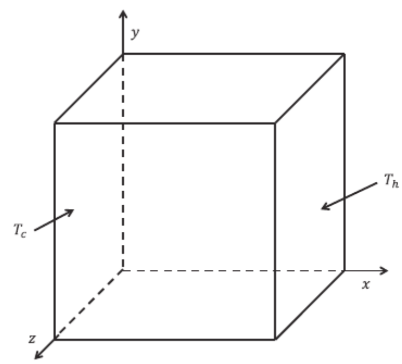

Fig. 7 *The physical domain of 3-D cubic model of Wang et al's study [44]*

The Wang et al. [44] benchmark was successfully replicated. Along the *x*-direction, the temperature profiles obtained for both models without radiation and the S2S and DO models were found to align closely with the CDUGKS simulations reported by Fusegi et al. [45], Krane and Jesse [46] and Wang et al [44] as shown in Fig. 8(a). Along the *y*-direction, the model without radiation aligned with the results from Fusegi et al. [45] and Wang et al. [44] study, but discrepancies are noted for the result obtained from the S2S and DO radiation model, which were observed to match the experimental measurements cited from Krane and Jesse [46] as shown in Fig. 8(b). Such agreements demonstrate that current works reliably capture both convective and radiative phenomena.

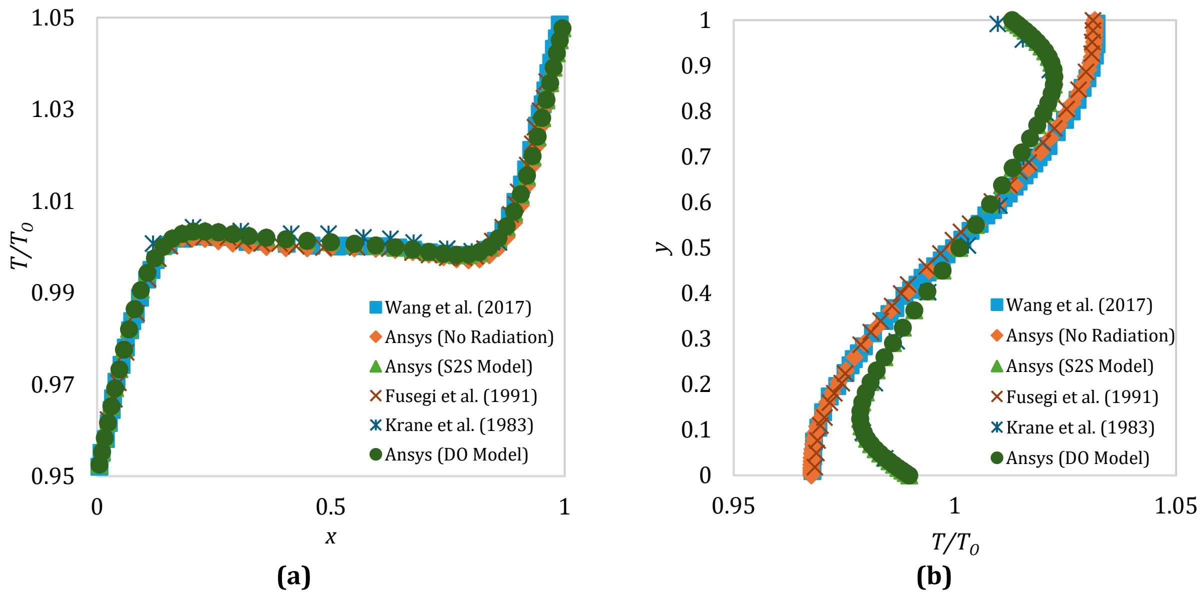

Fig. 8 *Comparison of the temperature distribution on the symmetry plane of (a) z = 0.5 (x vs T/To) and (b) z = 0.5 (y vs T/To) for model without radiation, S2S and DO radiation model against Fusegi et al. [45], Krane & Jessee [46] and Wang et al. [44]*

Collectively, the replication of Subiantoro & Ooi [43] FPSC cases and Wang et al.'s [44] cubical cavity benchmark established strong evidence of the accuracy and credibility of the current ANSYS Fluent setup. Although minor convergence challenges were encountered in the 3D solar collector model, the overall agreement with established benchmarks and experimental data was confirmed, indicating that this approach was well suited for the 3D framework.

3. Results and Discussions

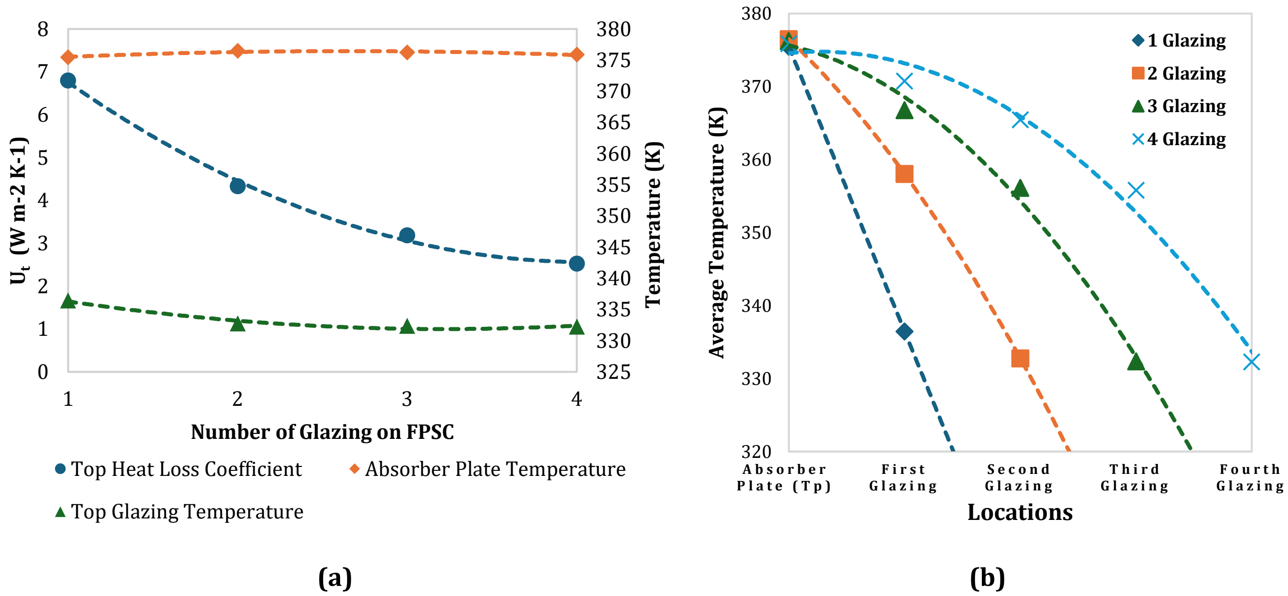

Fig. 9 *(a) The obtained value of the top heat loss coefficient, Ut.; (b) The average temperature of plate absorber, Tp and temperature of each glazing layers (Tg1, Tg2...)*

The top heat loss is quantified by the overall top heat loss coefficient, U_t, which represents the combined effects of convective and radiative heat transfer through the glazing system as expressed in Equations (1) and (16) to (18). For the current steady-state heat transfer with adiabatic conditions at the side walls and bottom wall, a lower U_t corresponds to reduced heat loss through convection and radiation; thus, a higher absorber temperature was expected.

Table 5 *Comparison of Ut across each configuration*

Configurations	Rate of change of U_t (%)
1-glazing to 2-glazing	36.28
2-glazing to 3-glazing	26.44
3-glazing to 4-glazing	20.80

The U_t was found to decrease with the addition of glazing layers as shown in Fig. 9(a). The rate of decrease of U_t between each glazing configuration is shown in Table 7. For instance, the U_t for a single glazing layer is 6.55 W m^{-2} K^{-1}, which drops significantly to 4.33 W m^{-2} K^{-1} for two layers, a 36.28 % reduction. Further additional glazing layer yields smaller incremental reductions, 26.44 % from two to three glazing, at 3.25 W m^{-2} K^{-1}, and only 20.80 % from three to four layers, at 2.62 W m^{-2} K^{-1}. This trend aligns with the assumption that U_t will decrease as more glazing layers are added. However, the rate of decline also starts to slow down, suggesting that the effect of decreasing U_t starts to diminish with increasing glazing layer. Based on the equation of U_t, adding more glazing creates more resistance, mainly in terms of h_c and h_r as shown in the extension of the equation from (1) and (16) to (18). Since these resistances are added in series, the total resistance becomes greater, and consequently, the inverse of the total resistance, which is the U_t will decrease.

In this numerical investigation, FPSC was modelled under steady-state conditions with a constant solar input and adiabatic side and bottom surfaces. The absorber plate temperature, T_p was utilised as an indirect indicator of top heat loss, hence overall collector performance. With controlled boundary conditions, with a constant solar input and adiabatic side and bottom surfaces, the absorber reached a steady-state temperature determined by the balance between absorbed solar energy and heat lost through the top surface via glazing. Under these conditions, A higher T_p implies reduced top heat loss, while a lower T_p indicates increased heat loss through the glazing layers. This approach is consistent with established research practices in which absorber temperature is the performance metric when heat losses are eliminated [7].

It is acknowledged that optical losses, reflection and absorption in the glazing layers can influence the overall energy balance. In this study, those optical effects were either explicitly modelled or assumed constant across all configurations, ensuring that any observed changes in absorber temperature are attributed primarily to differences in convective and radiative losses due to the number of glazing layers.

Under controlled boundary conditions, with the bottom and side walls set as adiabatic, only heat loss through the top surface occurs. Therefore, changes in absorber temperature reflect variations in top heat loss due to different glazing configurations. Fig. 9(b) shows the obtained average temperature of the plate absorber, T_p, and the temperature of each glazing layer, along with the trend for studying the number of glazing layers on the FPSC as measured in Ansys Fluent. The first glazing layer refers to the glazing layer at the bottom, nearest to the absorber plate, followed by subsequent glazing layers.

Figure 9(b) shows a non-linear trend in T_p as glazing layer increases 1-glazing configuration yields 375.46 K, 2-glazing peak at 376.48 K, 3-glazing plunge to 376.22 K, and 4-glazing decreases slightly to 375.87 K. This behaviour can be attributed to two opposing influences. First, each additional glazing and air gap raises the resistance, decreasing U_t while increasing T_p. Second, under the assumption of a refractive index of 1.5 for glazing, each new glazing traps more of the plate's long-wave infrared radiation and re-radiates it back, boosting the effective incident heat flux and tending to increase T_p.

At the 2-glazing layer, these effects balance so that the trapping of long-wave radiation outweighs the added insulation, driving T_p to its highest value. A third layer of glazing provides additional insulation, as indicated by the value of U_t, and significantly enhances the trapping of long-wave infrared radiation. However, it also leads to lower energy reaching the absorber plate due to optical losses, resulting in a slight reduction in T_p. Adding a fourth glazing tilts the balance toward optical losses, as the drop in T_p is observed, thus overtaking the incremental re-radiation.

In summary, the absorber temperature curve is characterised by the relation between minimised heat loss and improved thermal trapping. This simulation demonstrates that two glazing layers provide the best balance by reducing the amount of solar radiation lost during transmission. Any extra glazing mainly increases insulation, which alters the collector's energy balance and thus its operating temperature.

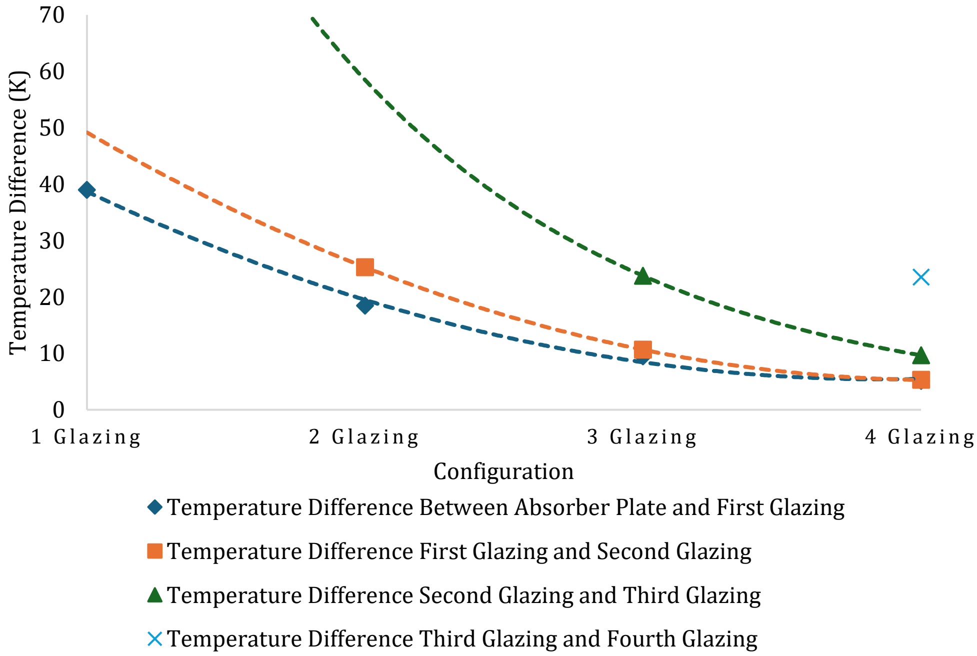

Fig. 10 *The trend of the temperature difference between the absorber plate and each successive glazing layer*

Fig. 10 shows that as the number of glazing layers increases, the temperature difference (ΔT) between all successive layers decreases consistently. This confirms that each additional glazing layer enhances insulation and diminishes heat loss. The temperature difference from the absorber plate to the first glazing layer decreases sharply as more glass layers are added. For the 1-glazing configuration, the temperature drops approximately 39.00 K, indicating significant heat transfer from the plate to the glazing. When two glazing layers are installed, the drop of the temperature between absorber plate and first glazing is cut approximately by half, to 18.45 K. Adding a third layer of glass reduces the drop to only 9.46 K, and with four glazing layers in place, the temperature change is very small, at only 5.12 K, indicating that glazing most effectively blocks heat from the plate at starting at 2- and 3-glazing layers configurations, but the effect diminishes for 4-glazing.

Optically, each glazing plays the role of transmitting the incoming short-wave solar radiation while reflecting or absorbing the long-wave radiation from the warmer surfaces below. As layers accumulate and the absorber plate and inner glazing have higher temperatures, as shown in Fig. 10, internal reflections and trapping of long-wave radiation intensify, further reducing net ΔT. Hence, the temperature drops are gradually distributed across the inner layers. For example, in the 4-glazing setup, the temperature drops across the first, second, and third air gap is around 5.12 K, 5.29 K, and 9.64 K, respectively, while the fourth gap drops significantly, about 23.53 K. The steepest temperature difference, therefore, shifts toward the outermost gap, highlighting that the final barrier to convective and radiative losses lies at the glass-air interface. Since the most significant thermal drop remains at the outermost layer, enhancements such as low-emissivity coatings or inert-gas fills in that gap can further reduce the total heat loss more effectively than simply adding more glass. While each additional glazing increases insulation, diminishing returns set in by the third or fourth glazing layer, so balancing these optical and thermal considerations yields the most cost-effective method to minimizing total top surface heat loss.

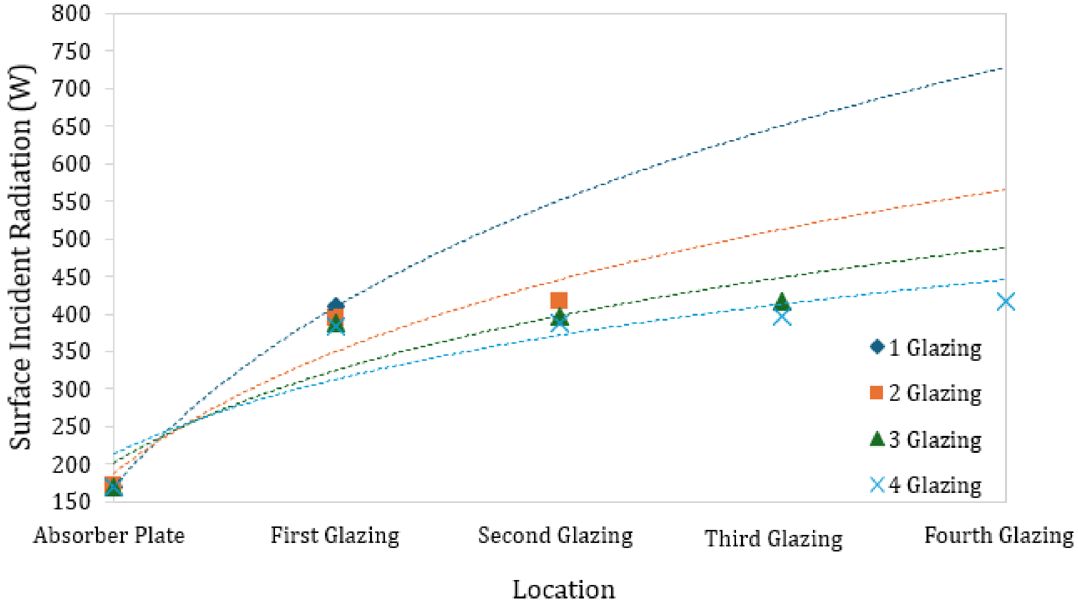

Fig. 11 *The surface incident radiation of absorber plate and each glazing layers, obtained from Anys Fluent*

Table 6 *The distribution of surface incident radiation of FPSC*

Surface Incident Radiation (W)	Absorber Plate	First Glazing	Second Glazing	Third Glazing	Fourth Glazing
Configuration:					
1-glazing	169.18	410.15	-	-	-
2-glazing	170.83	395.45	416.93	-	-
3-glazing	170.47	388.28	397.05	417.61	-
4-glazing	169.73	384.28	388.39	397.03	417.61

The distribution of incident radiation through the glazing is also influenced by the number of glazing layers. Assuming an ideal refractive index of 1.5, each glass layer transmits solar irradiance to the surfaces below. Adding more layers lengthens the radiative path and increases internal reflections within the glazing system, which can affect the amount of incident radiation reaching the interior surfaces.

Fig. 11 and Table 6 show that the surface incident radiation on the absorber plate peaks at the 2-glazing configuration and starts to decline gradually with the addition of glazing layers. When a second glazing layer is introduced, the absorber plate sees its highest net incident radiation because each glazing not only transmits the incoming short-wave solar beam but also traps a portion of the absorber's long-wave radiation due to the greenhouse effect. However, adding a third and fourth pane yields only a marginal benefit, as it slightly reduces the absorber's net incident radiation, because each extra glazing also causes optical loss, despite the greenhouse effect being slightly more significant. Thus, 2-glazing yields the best balance between enhanced long-wave re-radiation and minimized short-wave radiation losses.

Across all of the configurations, the outermost glazing has the highest incident radiation across all configurations, while each successive layer closer to the absorber shows a gradual decrease. Every glazing surface both reflects the incoming beam and exchanges radiation with its neighbors. Some of the radiation reflected back down from the hotter lower surfaces will be intercepted by the glazing above, increasing their net incident beyond just the direct sunlight.

Although each additional glazing lowers U_t by improving insulation and increases the share of radiation trapped among the glazing itself due to the greenhouse effect, it also introduces more optical losses. From a performance and cost-benefit standpoint, two layers appear to strike the best balance between minimizing top heat losses and maximizing radiative input to the absorber as discussed.

In summary, the balance between U_t and surface incident radiation explains why 2-glazing yields the highest absorber temperature. It achieves an optimal greenhouse effect by trapping long-wave radiation, while still maintaining relatively low optical losses as well as enhanced thermal insulation from lower U_t. By contrast, 3-and 4-glazing shift the balance further toward greenhouse effect enhancement, but it also yields increasing optical losses. The single-glazing setup, with the highest U_t and lowest incident radiation, clearly underperforms, resulting in the lowest absorber temperature.

Future enhancements such as low-emissivity coatings on the outermost glazing, anti-reflective treatments on inner glazing, or vacuum glazing or argon-filled cavities can further improve the performance of FPSC.

4. Conclusion

In this study, the interaction between the number of glazing layer configurations, top heat loss, absorber temperature, and internal radiation was systematically examined under ideal optical conditions. As glazing layers increase, the overall top heat loss coefficient, U_t falls sharply, confirming that each additional air gap and glazing adds significant thermal resistance via convection and radiation insulation. Additionally, adding more glazing enhances the greenhouse effect by trapping long-wave thermal radiation, but also introduces additional optical losses due to increased internal reflections at each glazing layer.

The optimal FPSC design therefore requires carefully balancing the number of glazing layers to lower the Ut while taking advantage of the greenhouse effect as well as minimising short-wave optical losses in order to achieve balanced FPSC performance. These insights underscore the importance of optimizing both thermal and optical properties in FPSC design in Malaysia's hot climate. By carefully selecting the number of glazing layers and integrating advanced materials and configurations, future collectors can achieve a more efficient balance between minimizing thermal losses and maximizing solar energy capture.

Acknowledgement

The authors would like to acknowledge the support of International Islamic University Malaysia, in particular the Department of Mechanical and Aerospace Engineering, for carrying out this study.

Conflict of Interest

The authors declare that there is no conflict of interest regarding the paper's publication.

Author Contribution

The authors confirm contribution to the paper as follows: ***study conception and design:*** *Akeef Mursyidiy, Dr. Syed Noh;* ***data collection:*** *Akeef Mursyidiy;* ***analysis and interpretation of results:*** *Akeef Mursyidiy, Dr. Syed Noh;* ***draft manuscript preparation:*** *Akeef Mursyidiy, Syed Noh Syed Abu Bakar, Sany Izan Ihsan, Mohd Azan Mohammed Sapardi, and Mohammad Jamil Ahmad. All authors reviewed the results and approved the final version of the manuscript.*

References

[1] M. Hoel and S. Kverndokk, "Depletion of fossil fuels and the impacts of global warming," *Resour Energy Econ*, vol. 18, no. 2, pp. 115–136, Jun. 1996, https://doi.org/10.1016/0928-7655(96)00005-X.

[2] A. O. M. Maka and J. M. Alabid, "Solar energy technology and its roles in sustainable development," *Clean Energy*, vol. 6, no. 3, pp. 476–483, Jun. 2022, https://doi.org/10.1093/ce/zkac023.

[3] R. P. Thombs, "The asymmetric effects of fossil fuel dependency on the carbon intensity of well-being: A U.S. state-level analysis, 1999–2017," *Global Environmental Change*, vol. 77, p. 102605, Nov. 2022, https://doi.org/10.1016/J.GLOENVCHA.2022.102605.

[4] V. E. Dudley, C. W. Matthews, and L. R. Evans, "Test result industrial solar technology PTC," 1995.

[5] S. Kalogirou, "The potential of solar industrial process heat applications," *Appl Energy*, vol. 76, no. 4, pp. 337–361, Dec. 2003, https://doi.org/10.1016/S0306-2619(02)00176-9.

[6] W. B. Stine, "Progress in parabolic dish technology," 1989.

[7] S. A. Kalogirou, "Solar thermal collectors and applications," 2004. https://doi.org/10.1016/j.pecs.2004.02.001.

[8] A. Kumar, Z. Said, and E. Bellos, "An up-to-date review on evacuated tube solar collectors," *J Therm Anal Calorim*, vol. 145, Jun. 2020, https://doi.org/10.1007/s10973-020-09953-9.

[9] R. Roy, "COMPARISON OF COMMERCIAL AND DO-IT-YOURSELF SOLAR COLLECTORS 'Don't invest in anything that eats or needs repainting' O liver Wendell Holmes," 1979.

[10] L. A. Omeiza *et al.*, "Application of solar thermal collectors for energy consumption in public buildings – An updated technical review," *Journal of Engineering Research*, vol. 12, no. 4, pp. 994–1010, Dec. 2024, https://doi.org/10.1016/J.JER.2023.09.011.

[11] O. S. Idowu and O. M. Olarenwaju, "Determination of optimum tilt angles for solar collectors in low-latitude tropical region," 2013. [Online]. Available: http://www.journal-ijeee.com/content///

[12] A. Kocer, I. Yaka, G. Sardogan, and A. Gungor, "Effects of Tilt Angle on Flat-Plate Solar Thermal Collector Systems," *Br J Appl Sci Technol*, vol. 9, no. 1, pp. 77–85, Jan. 2015, https://doi.org/10.9734/bjast/2015/17576.

[13] Y. Lv, P. Si, X. Rong, J. Yan, Y. Feng, and X. Zhu, "Determination of optimum tilt angle and orientation for solar collectors based on effective solar heat collection," *Appl Energy*, vol. 219, pp. 11–19, Jun. 2018, https://doi.org/10.1016/J.APENERGY.2018.03.014.

[14] G. Barone, A. Buonomano, C. Forzano, and A. Palombo, "Solar thermal collectors," *Solar Hydrogen Production: Processes, Systems and Technologies*, pp. 151–178, Jan. 2019, https://doi.org/10.1016/B978-0-12-814853-2.00006-0.

[15] N. Akhtar and S. C. Mullick, "Effect of absorption of solar radiation in glass-cover(s) on heat transfer coefficients in upward heat flow in single and double glazed flat-plate collectors," *Int J Heat Mass Transf*, vol. 55, no. 1–3, pp. 125–132, Jan. 2012, https://doi.org/10.1016/j.ijheatmasstransfer.2011.08.048.

[16] R. Bakari, R. J. A. Minja, and K. N. Njau, "Effect of Glass Thickness on Performance of Flat Plate Solar Collectors for Fruits Drying," *Journal of Energy*, vol. 2014, pp. 1–8, 2014, https://doi.org/10.1155/2014/247287.

[17] N. Ehrmann and R. Reineke-Koch, "Selectively coated high efficiency glazing for solar-thermal flat-plate collectors," *Thin Solid Films*, vol. 520, no. 12, pp. 4214–4218, Apr. 2012, https://doi.org/10.1016/J.TSF.2011.04.094.

[18] F. Giovannetti, S. Föste, N. Ehrmann, and G. Rockendorf, "High transmittance, low emissivity glass covers for flat plate collectors: Applications and performance," *Solar Energy*, vol. 104, pp. 52–59, Jun. 2014, https://doi.org/10.1016/J.SOLENER.2013.10.006.

[19] N. Ihaddadene, R. Ihaddadene, and A. Mahdi, "Effect of Glazing Number on the Performance of a Solar Thermal Collector," 2014. [Online]. Available: www.ijsr.net

[20] M. Khoukhi, S. Maruyama, A. Komiya, and M. Behnia, "Flat-plate solar collector performance with coated and uncoated glass cover," *Heat Transfer Engineering*, vol. 27, no. 1, pp. 46–53, Jan. 2006, https://doi.org/10.1080/01457630500343009.

[21] D. Sarma, P. Bakul, B. 2#, D. Hatibaruah, and M. E. Student, "Optimization of Glazing Cover Parameters of a Solar Flat Plate Collector (FPC)," *International Journal of Engineering Trends and Technology*, vol. 14, no. 2, 2014, [Online]. Available: http://www.ijettjournal.org

[22] T. H. Patrick, T. F. Abraham, E. Marcel, and K. Alexis, "Numerical study of the greenhouse effect in a flat-plate double glazing solar heat collector," *Indian J Sci Technol*, vol. 12, no. 38, pp. 1–9, Oct. 2019, doi: 10.17485/ijst/2019/v12i38/145315.

[23] S. A. Al-Ajlan, H. Al Faris, and H. Khonkar, "A simulation modeling for optimization of flat plate collector design in Riyadh, Saudi Arabia," *Renew Energy*, vol. 28, no. 9, pp. 1325–1339, 2003, https://doi.org/10.1016/S0960-1481(02)00254-9.

[24] C. Q. Chen *et al.*, "Numerical evaluation of the thermal performance of different types of double glazing flat-plate solar air collectors," *Energy*, vol. 233, p. 121087, Oct. 2021, https://doi.org/10.1016/J.ENERGY.2021.121087.

[25] M. Ameri, H. Farzan, and M. Nobari, "Evaluation of Different Glazing Materials, Strategies, and Configurations in Flat Plate Collectors Using Glass and Acrylic Covers: An Experimental Assessment," *Iranian Journal of Energy and Environment*, vol. 12, no. 4, pp. 273–284, 2021, https://doi.org/10.5829/ijee.2021.12.04.01.

[26] D. Arasteh, P. E. S. Selkowitz, and J. Hartmann, "DETAILED THERMAL PERFORMANCE DATA ON CONVENTIONAL AND HIGHLY INSULATING WINDOW SYSTEMS," 1985.

[27] Y. Nassar *et al.*, "Optimum Number of Glass Covers of Thermal Flat Plate Solar Collector," 2024.

[28] P. N. Givi, L. Arazipooor, L. Arazipoor, and S. P. Hosseini, "CFD Analysis Of Mass Flow And Glass Cover Thickness To Improve Solar Air Collector Performance," 2025, https://doi.org/10.56726/IRJMETS67551.

[29] Y. Liu, C. Tan, Y. Jin, and S. Ma, "Heat collection performance analysis of corrugated flat plate collector: An experimental study," *Renew Energy*, vol. 181, pp. 1–9, Jan. 2022, https://doi.org/10.1016/J.RENENE.2021.09.001.

[30] S. Singh*, Dr. U. Gupta, and Dr. A. Bansal, "Performance of Flat Plate Solar Collectors using Different Thickness of Glazing Material," *International Journal of Recent Technology and Engineering (IJRTE)*, vol. 8, no. 6, pp. 5787–5793, Mar. 2020, https://doi.org/10.35940/ijrte.F8480.038620.

[31] M. Harun *et al.*, "Study on Selection of a Suitable Material and The Parameters for Designing a Portable Flat Plate Base-Thermal Cell Absorber (FPBTCA)," *Journal of Advanced Research in Fluid Mechanics and Thermal Sciences*, vol. 85, pp. 71–92, Jul. 2021, https://doi.org/10.37934/arfmts.85.1.7192.

[32] X. Wang *et al.*, "Parametric Study and Optimization of a New Type of Solar Air Collector Employing Flat Micro Heat Pipe Arrays," *J Therm Sci Eng Appl*, vol. 17, no. 3, Jan. 2025, https://doi.org/10.1115/1.4067633.

[33] N. M. Nahar and H. P. Garg, "Free convection and shading due to gap spacing between an absorber plate and the cover glazing in solar energy flat-plate collectors," *Appl Energy*, vol. 7, no. 1–3, pp. 129–145, Nov. 1980, https://doi.org/10.1016/0306-2619(80)90054-9.

[34] N. M. Nahar and J. P. Guf'ta, "Studies On Gap Spacing Between Absorber and Cover Glazing In Flat Plate Solar Collectors Free Convection Shading Air gap Flat-plate Collector Solar energy," 1989.

[35] F. Pourfayaz, R. Shirmohammadi, A. Maleki, and A. Kasaeian, "Improvement of solar flat-plate collector performance by optimum tilt angle and minimizing top heat loss coefficient using particle swarm optimization," *Energy Sci Eng*, vol. 8, no. 8, pp. 2771–2783, Aug. 2020, https://doi.org/10.1002/ese3.693.

[36] Y. Wenceslas Koholé, F. Cyrille Vincelas Fohagui, and G. Tchuen, "Flat-plate solar collector thermal performance assessment via energy, exergy and irreversibility analysis," *Energy Conversion and Management: X*, vol. 15, p. 100247, Aug. 2022, https://doi.org/10.1016/J.ECMX.2022.100247.

[37] A. Mekahlia, L. Boumaraf, and C. Abid, "CFD analysis of the thermal losses on the upper part of a flat solar collector," *Heat Transfer*, vol. 49, no. 5, pp. 2921–2942, Jul. 2020, https://doi.org/10.1002/htj.21753.

[38] S. K. Samdarshi and S. C. Mullick, "An Improved Technique for Computing the Top Heat Loss Factor of a Flat-Plate Collector With a Single Glazing," 1988. [Online]. Available: http://solarenergyengineering.asmedigitalcollection.asme.org/

[39] A. Bisen, P. P. Dass, and R. Jain, "Parametric studies of top heat loss coefficient of double glazed flat plate solar collectors," *MIT Int J Mech Eng*, vol. 1, no. 2, pp. 71–78, 2011.

[40] W. C. Swinbank, "Long-wave radiation from clear skies," 1963.

[41] H. Buchberg, I. Cation, and D. K. Edwards, "Natural Confection in Enclosed Spaces-A Review of Application to Solar Energy Collection," 1976. [Online]. Available: http://heattransfer.asmedigitalcollection.asme.org/

[42] S. C. Mullick and Samdarshi S K, "S. K. Samdarshi Analytical Equation for the Top Heat Loss Factor of a Flat-Plate Collector With Double Glazing," 1991. [Online]. Available: http://solarenergyengineering.asmedigitalcollection.asme.org/

[43] A. Subiantoro and K. T. Ooi, "Analytical models for the computation and optimization of single and double glazing flat plate solar collectors with normal and small air gap spacing," *Appl Energy*, vol. 104, pp. 392–399, Apr. 2013, https://doi.org/10.1016/J.APENERGY.2012.11.009.

[44] P. Wang, Y. Zhang, and Z. Guo, "Numerical study of three-dimensional natural convection in a cubical cavity at high Rayleigh numbers," *Int J Heat Mass Transf*, vol. 113, pp. 217–228, 2017, https://doi.org/10.1016/j.ijheatmasstransfer.2017.05.057.

[45] T. Fusegi, J. M. Hyun, K. Kuwahara, and B. Farouk, "A numerical study of three-dimensional natural convection in a differentially heated cubical enclosure," *Int J Heat Mass Transf*, vol. 34, no. 6, pp. 1543–1557, Jun. 1991, https://doi.org/10.1016/0017-9310(91)90295-P.

[46] R. J. Krane and J. Jessee, "Some Detailed Field Measurements for a Natural Convection Flow in a Vertical Square Enclosure," in *Proceedings of the First ASME-JSME Thermal Engineering Joint Conference*, Hawaii, USA, Mar. 1983, pp. 323–329.